photonics

MDPI

Article

The Rapid Detection of Paclitaxel-Induced Changes in Cervical Cancer Cells Using an Ultrasensitive Biosensor

Liwen Zhang [1,†], Gan Chen [2,†], Yating Hao [2] and Yan Peng [2,*]

[1] Department of Gynecology, Yueyang Hospital of Integrated Traditional Chinese and Western Medicine, Shanghai University of Traditional Chinese Medicine, Shanghai 200080, China; yy210025@shutcm.edu.com
[2] Terahertz Technology Innovation Research Institute, Terahertz Spectrum and Imaging Technology Cooperative Innovation Center, Shanghai Key Lab of Modern Optical System, University of Shanghai for Science and Technology, Shanghai 200093, China; cg1@usst.edu.cn (G.C.); 222302361@st.usst.edu.cn (Y.H.)
* Correspondence: py@usst.edu.cn
† These authors contributed equally to this work.

Abstract: Background: Paclitaxel is a widely used cancer treatment drug that has a significant inhibitory effect on cervical cancer cells (HeLa cells). This study aims to investigate the effects of paclitaxel on HeLa cells and evaluate the application of terahertz (THz) spectroscopy and surface plasmon resonance (SPR) biosensors in this process. Methods: We utilized an SPR biosensor in conjunction with THz spectroscopy to measure the terahertz absorbance spectra of HeLa cells exposed to various concentrations of paclitaxel. The minimum number of cells used for detection was 15.25×10^5. At the same time, cell proliferation levels were assessed through proliferation assays and compared with the terahertz spectroscopy data. Results: The experimental results indicated that with the increasing concentration of paclitaxel, the terahertz absorbance spectra of HeLa cells exhibited a blue shift, and cell proliferation was significantly inhibited. The results of the proliferation assays were consistent with the terahertz spectroscopy data, validating the effectiveness of this method. Conclusion: This study demonstrates that the combination of THz spectroscopy and SPR biosensors is a promising technology that can provide a simple, rapid, and low-cost method for studying chemistry–biology relationships, especially in the field of drug evaluation.

Keywords: terahertz spectroscopy; paclitaxel; surface plasmon resonance biosensors

Citation: Zhang, L.; Chen, G.; Hao, Y.; Peng, Y. The Rapid Detection of Paclitaxel-Induced Changes in Cervical Cancer Cells Using an Ultrasensitive Biosensor. *Photonics* **2024**, *11*, 735. https://doi.org/10.3390/photonics11080735

Received: 8 July 2024
Revised: 31 July 2024
Accepted: 31 July 2024
Published: 7 August 2024

1. Introduction

Cervical cancer remains a major global health problem, ranking as the fourth most common cancer in women. Moreover, 85% of cases and 90% of deaths are in low- and middle-income countries [1]. In contrast, developed nations have seen a decline in both prevalence and mortality rates due to extensive screening and vaccination programs, although cervical cancer continues to be a leading gynecological malignancy [2,3].

Primary treatments for cervical cancer include surgical procedures, chemotherapy, and radiotherapy, with chemotherapy being widely used. Paclitaxel, one of the most effective anticancer drugs, inhibits cancer cell growth by inducing cell cycle arrest and mitotic failure [4–7]. It also triggers various forms of cell death, including mitotic catastrophe and the activation of pro-apoptotic mediators, while influencing anti-apoptotic mediators [8]. Since its discovery, paclitaxel has treated over one million patients, making it a prevalent anticancer agent [9].

In cancer research, cell strains are extensively used as in vitro models for biochemical characterization, diagnosis, and therapeutic development. The Hela cervical cancer cell line, in particular, has been a cornerstone in cancer research, serving as a classical human immortalized cell line across various research domains [10,11]. Among these, the Hela cervical cancer cell line has been particularly significant, serving as a classical human immortalized cell line across various research domains [12,13]. Traditional methods for identifying these

cells include morphological assessments, immunohistochemistry, isoenzyme assays, and karyotyping [14–17]. While effective, these methods are often labor intensive and time consuming, requiring multiple pre-treatments and supplementary indicators or reagents. Recent advancements have introduced terahertz (THz) wave-based techniques as promising tools in biomedical research. THz waves, lying between the microwave and infrared ranges of the spectrum, with frequencies from 0.1 to 10 THz offer a non-destructive means for tissue and cell analysis [18,19]. Our novel approach combines terahertz spectroscopy with a metamaterial-based terahertz biosensor to quantitatively detect cancer cells [20,21]. This biosensor detects alterations in the surface dielectric constant, causing a corresponding shift in the resonance frequency [22]. By interpreting these frequency shifts relative to different sample contents, we can quantitatively analyze target substances [23–25].

In this research, we explored the effects of paclitaxel on HeLa cells using SPR biosensors integrated with THz-TDS. We assessed cell survival rates after exposure to different drug concentrations, utilizing the CCK-8 assay and MTT. This approach offers a novel perspective on drug–cell interactions via terahertz spectroscopy.

2. Materials and Methods

2.1. Sample Preparation

2.1.1. Cell Culture

The HeLa cervical cancer cell strain, sourced from the Chinese National Infrastructure of Cell Line Resource in Beijing, was maintained in RPMI 1640 medium with the addition of 10% fetal bovine serum and 1% penicillin–streptomycin. The cells were kept in a CO_2 incubator at 37 °C with 5% CO_2 atmosphere.

2.1.2. Reagents

Paclitaxel was acquired from Yuan Ye Biological Co. (Shanghai, China). Reagent preparation followed the manufacturer's protocols strictly, and paclitaxel stock solutions were preserved at 4 °C.

2.1.3. Terahertz Sample Preparation

Upon reaching the logarithmic growth phase, HeLa cells were washed twice with sterile PBS (phosphate-buffered saline). We then added 1 mL of 0.25% trypsin solution containing 0.02% EDTA (ethylenediaminetetraacetic acid) to the culture medium. Once the cells were adequately dissociated through gentle agitation, 5 mL of fresh medium with 10% FBS (fetal bovine serum) was added to stop the trypsin activity. The cell and trypsin mixture was centrifuged at 1000 rpm for 5 min in a sterile environment, The supernatant was removed, and the cells were then resuspended in fresh medium. A cell count was performed three times using 20 µL of the cell suspension, with counts averaged to determine the concentration. The cell suspension was adjusted to a final concentration of 5×10^6 cells/mL. Following an 80 min incubation to allow cell adherence and the removal of non-adherent dead cells, the cells were fixed with 95% ethanol at room temperature for 30 min and centrifuged again. The resuspension was carried out using 95% ethanol, with 5 µL of the cell suspension placed on microarrays and left to dry. The whole process can be seen in the schematic diagram in Figure 1. Two concentrations of cell suspension were prepared: 5×10^6 cells/mL and 5×10^5 cells/mL.

2.1.4. Cell Viability Assay

Before assessing cell viability, HeLa cells were exposed to paclitaxel at concentrations between 5 and 100 nM for a duration of 24 h. The viability of the cells was evaluated using the Cell Counting Kit-8 (CCK-8) assay. HeLa cells were plated into 96-well plates at a density of 3×10^3 cells per well. After an overnight incubation, the medium was replaced with fresh medium containing the designated concentrations of paclitaxel for 24 h. Following this treatment period, 10 µL of CCK-8 reagent was added to each well, and the plates were incubated for an further 2 h. The optical density (OD) was then measured at

450 nm using the Epoch Microplate Reader (BioTek, Winooski, VT, USA). Cell viability was determined using the following formula: cell viability (%) = (OD of treatment − OD of blank control)/(OD of control − OD of blank control) × 100%.

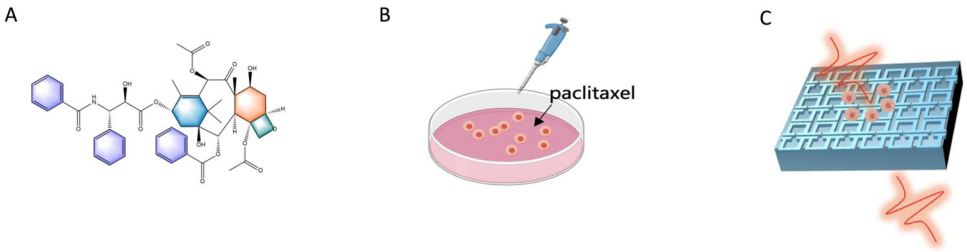

Figure 1. Structural formula of paclitaxel. (**A**) Schematic of cellular incorporation of paclitaxel (**B**). Terahertz workflow diagram (**C**).

An additional cell viability assay, the MTT assay, was also conducted. HeLa cells were initially seeded at a density of 5000 cells per well in a 96-well plate. After incubating for 24 h, the cells were treated with varying concentrations of paclitaxel for 48 h. Post treatment, the medium was removed, and 100 µL of MTT reagent (0.5 mg/mL) was added to each well. The cells were then incubated for 4 h. After incubation, the MTT solution was replaced with 100 µL of DMSO to solubilize the formazan crystals formed. Absorbance was read at 570 nm, with background correction performed at 630 nm. Cell viability was quantified relative to untreated controls, with the results averaged from three independent experiments.

2.2. Terahertz Spectroscopy System

The Advantest TAS7400 spectrometer utilizes two ultra-short pulse lasers, denoted as A and B, which operate in tandem. The A laser directs a femtosecond pulse through a fiber optic to a terahertz (THz) emitter, initiating THz pulse generation via a photoconductive antenna under an external electric field. These THz pulses, once formed, are directed through an optical lens and interact with the sample, thus embedding the sample's information within them. Simultaneously, the B laser emits a pulse that travels alongside the THz signal in an electro-optic crystal, leveraging the crystal's birefringence to encode the sample's data onto the detection pulse. The decoding of the sample's THz spectrum is achieved using free-space electro-optic sampling, with the signal being digitized and then transformed via fast Fourier transform for spectral analysis (Figure 2). The system, boasting a dynamic range exceeding 60 dB, functions optimally within a THz range of 0.5 to 4 THz and features a spectral resolution near 1.9 GHz. Its THz emitter is energized by a pump laser delivering an output of 20 mW, at a central wavelength of 1550 nm, and pulse duration of 50 fs. For thorough analysis, each sample undergoes four measurements, totaling 12 min per sample [26].

2.3. SPR Biosensor

Our study utilizes a custom-designed SPR biosensor, employing gold for resonance and quartz as the substrate [27]. The metasurfaces, coated with chromium and gold films on polished quartz, are patterned by traditional photolithography, utilizing chromium as an adhesion layer. The substrate's thickness stands at 500 µm. Within the biosensor, dipole resonance induces an electric field concentrated mainly in the resonant cavity and along its perimeter, creating a toroidal field in a clockwise pattern. The magnetic field enhancement for dipole resonance occurs near the resonant cavity's surface. We also investigated the oblique incident wave's impact on absorption spectra. Utilizing a commercially available system with an incident angle range of -10° to 10°, our analysis encompasses resonant responses at angles from -20° to 20°, revealing that oblique angles do not significantly alter absorption spectra. This biosensor system effectively quantifies small molecules by measuring resonance frequency shifts, which correspond to variations in sample dielectric

constants, facilitating the targeted substance's quantitative detection and analysis through frequency shift mapping.

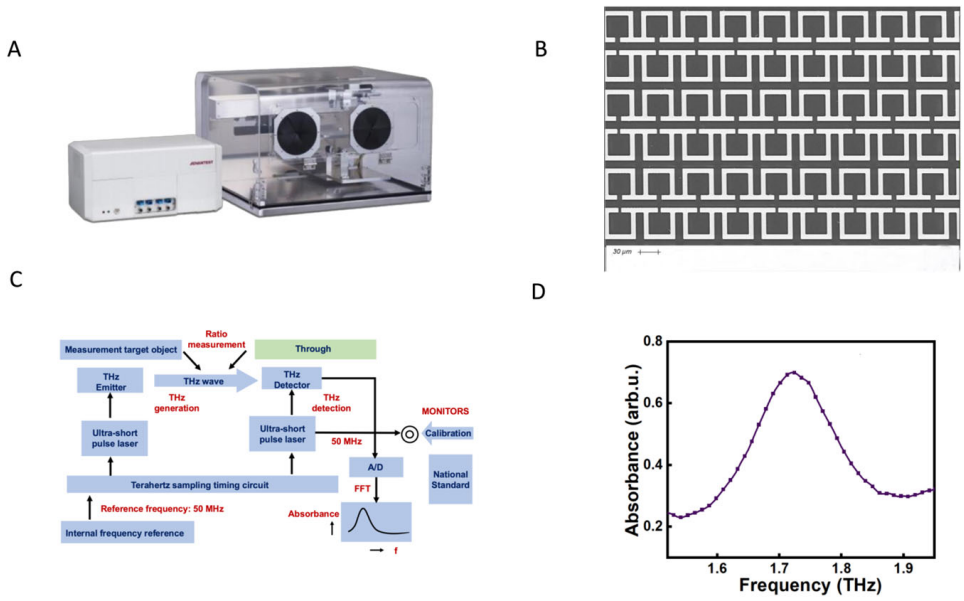

Figure 2. Terahertz time-domain spectrometer TAS7400SP (**A**). SEM image of the device (**B**). Diagram of the internal workings of the THz-TDS (TAS7400SP) (**C**). Absorption diagram of the RTA (**D**).

2.4. Data Processing and Analysis

Data analysis was performed with Matlab 2021 and Origin 2021b software suites. Terahertz time−domain spectroscopy (TDS) samples were tested in quadruplicate to ensure accuracy. Collected data were imported into Matlab for averaging and peak value determination, then analyzed in Origin for further insight. Baseline biosensor readings without samples established the initial peak values, from which subsequent sample readings were subtracted for comparison. All samples were subjected to at least three independent experiments, and data were presented as average values accompanied by standard deviations. Statistical significance was determined using a two-sample *t*-test performed in Origin Pro 8.5. A *p*-value of less than 0.05 was considered indicative of significant difference.

3. Result and Discussion

3.1. Viability of Hela Cells

This research examined the link between terahertz absorption coefficients and indicators of cellular health using CCK−8 and MTT assays. Both assays evaluate cell proliferation and metabolic activity, with CCK−8 providing higher sensitivity compared to MTT. These methods are widely recognized for assessing cellular responses to drug treatments [28–30]. Previous studies have reported a reduction in HeLa cell viability with increasing paclitaxel concentrations, leading us to test a range from 0 to 100 nM. Data presented in Figure 3A,B,D,E indicate that HeLa cell viability was notably reduced at paclitaxel concentrations of 20–100 nM relative to the untreated controls. Both CCK−8 and MTT assays corroborated this finding, showing a consistent decrease in viability with higher paclitaxel concentrations. Data presented in Table 1.

3.2. Terahertz Spectroscopy Investigation into the Effects of Paclitaxel on HeLa Cells

In this research, we focused on assessing the response of HeLa cells to paclitaxel at concentrations from 0 nM to 100 nM. For SPR biosensor analysis, we utilized a 5 µL aliquot of the evenly dispersed cell suspension and measured absorbance with THz−TDS across the 0.5−4 THz frequency range. Figure 4A shows the differential absorbance of the cell solution after paclitaxel treatment, with zoomed-in sections in Figure 4A illustrating changes in peak

positions. The average frequency values for each paclitaxel concentration were calculated at concentrations of 0 nM (1.7209 THz), 5 nM (1.7252 THz), 10 nM (1.7314 THz), 20 nM (1.7343 THz), 40 nM (1.7424 THz), 80 nM (1.7452 THz), and 100 nM (1.7471 THz). The relevant information is shown in Table 2.

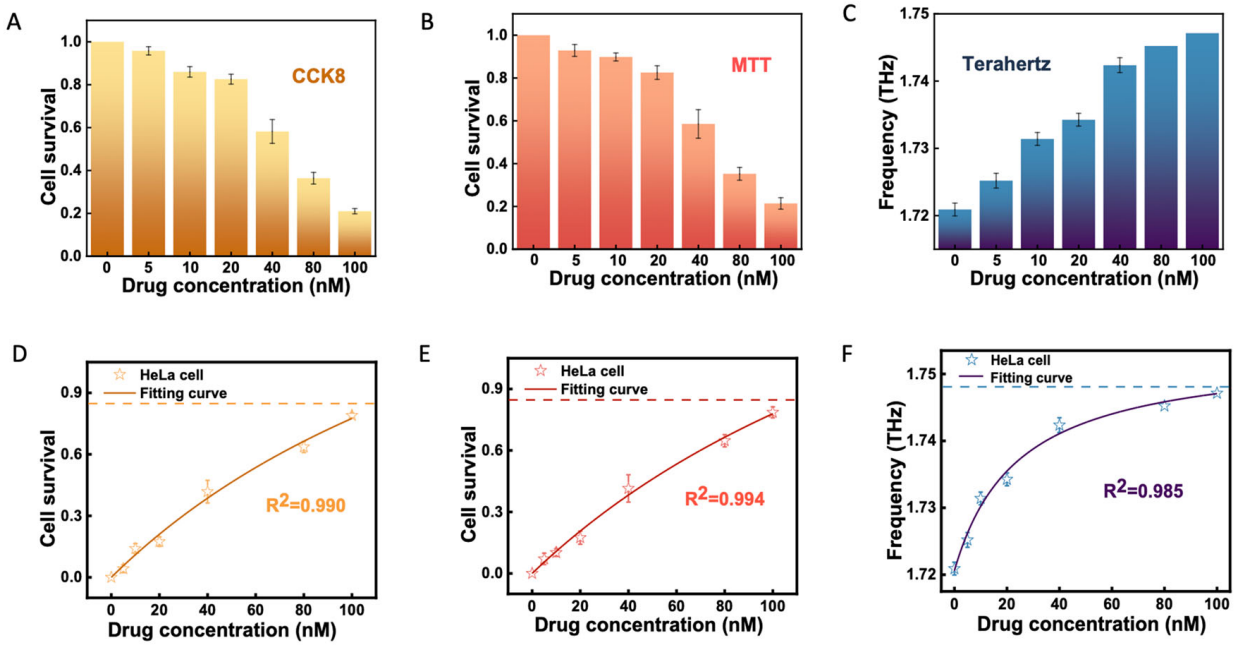

Figure 3. Cell viability test (**A**,**B**). Effect of drug levels on the survival of HeLa cells (**D**,**E**) and corresponding frequency shift as a function (**C**), with a bar graph of the corresponding frequency shifts (**F**) for various paclitaxel concentrations in HeLa cells.

Table 1. Viability of Hela cells.

Viability of Hela Cells				
Drug Concentration (nM)	**CCK8 Mean**	**CCK8 SE**	**MTT Mean**	**MTT SE**
0	1	0	1	0
5	0.958	0.01924	0.929	0.02794
10	0.86	0.02449	0.8984	0.01878
20	0.826 *	0.02302	0.8256 *	0.03188
40	0.582 **	0.05541	0.5854 **	0.06668
80	0.364 **	0.02702	0.3524 **	0.02975
100	0.21 **	0.01225	0.214 **	0.02687

* $p < 0.05$, ** $p < 0.01$.

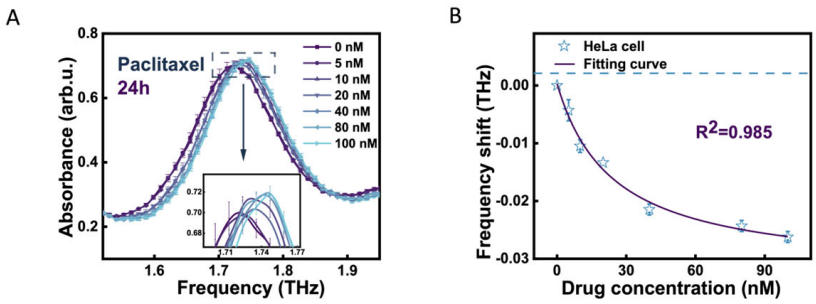

Figure 4. Spectra of absorbance (**A**). Magnified portion of absorbance spectra (**B**).

Table 2. Terahertz spectroscopy analysis.

Terahertz Spectroscopy Analysis of Paclitaxel Effect on HeLa Cells							
Drug Concentration (nM)	0	5	10	20	40	80	100
Frequency	0	0.071	0.1016	0.1744	0.4146	0.6476	0.786
Standard Error	0	0.02794	0.01878	0.03188	0.06668	0.02975	0.02687

Figure 4B presents a graph that elucidates the correlation between the shifts in hypersurface resonance peak frequencies and the cytosolic samples' cell counts post paclitaxel treatment. It is evident that the hypersurface resonance peak's frequency shift is inversely proportional to the cell quantity; a decrease in cell count results in the SPR biosensor's resonance peak shifting to higher frequencies with increased paclitaxel concentrations. We derived the frequency shift data for each cytosolic sample to chart the relationship relative to paclitaxel levels, using the following fitting equation:

$$y = -Vmax * x/(Km + x) + a \quad (1)$$

The detailed formula is as follows:

$$MTT: y = (2.535 \pm 0.609)x/[(225.236 \pm 73.339) + x]$$

$$CCK8: y = (2.360 \pm 0.663)x/[(204.400 \pm 79.654) + x]$$

$$THz: y = (0.033 \pm 0.002)x/[(24.157 \pm 5.449) + x]$$

In this equation, x indicates the administered paclitaxel concentration, y represents the frequency shift observed by the terahertz SPR biosensor, Vmax is the highest frequency shift, and Km corresponds to the paclitaxel concentration at half the maximal frequency shift.

To clarify our findings, we extracted the average frequency values at varying concentrations to perform curve fitting. The resultant plots, depicted in Figure 3C, articulate the correlation between these average frequency values and the paclitaxel concentrations. Figure 3F shows the data fitting used to establish the connection with paclitaxel concentration, utilizing the following formula:

$$y = Vmax * x/(Km + x) + a \quad (2)$$

This technique illustrates the connection between drug concentration and the resulting frequency shifts on the biosensor.

3.3. Morphology of HeLa Cells

Paclitaxel treatment led to changes in the density of Hela cells. In our experiments, we observed that different concentrations of paclitaxel had significant effects on the morphology and density of Hela cells. Untreated Hela cells formed a monolayer cell structure (Figure 5A), while Hela cells treated with various concentrations of paclitaxel (Figure 5B) showed similar morphology to the untreated cells but with gradually decreasing density. However, when Hela cells were treated with 40 nM paclitaxel (Figure 5E), the cell density was significantly reduced, and the cell morphology became more rounded, indicating signs of inhibited cell growth. As the dosage of paclitaxel increased, its effect on inhibiting the growth of Hela cells became more pronounced. This phenomenon is consistent with other observations that high-dose paclitaxel exposure leads to apoptosis in cells [31].

Additionally, studies have shown that paclitaxel can inhibit the growth of various cancer cell lines by inducing apoptosis and inhibiting cell proliferation Our results further confirm these previous findings, indicating that paclitaxel has a significant effect on inhibiting the growth of Hela cells. These findings not only provide new insights into the mechanism of action of paclitaxel but also offer a theoretical basis for its application in cancer treatment in the future.

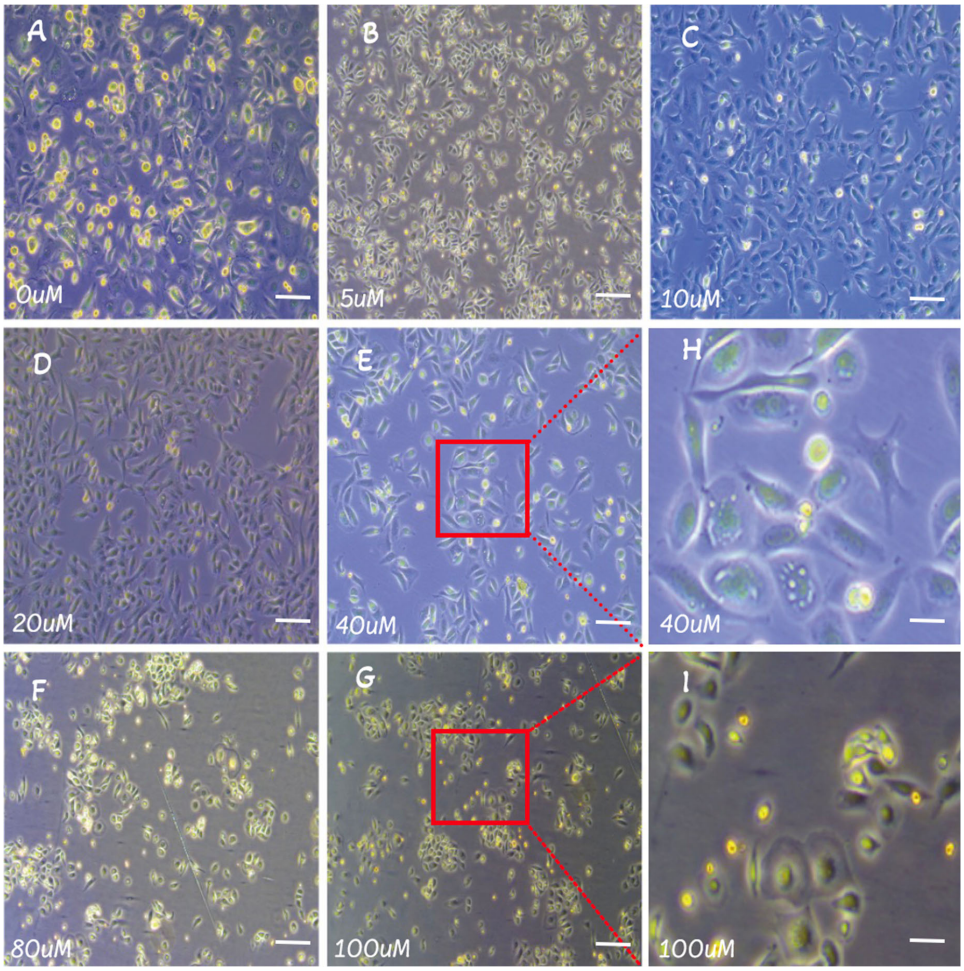

Figure 5. The morphological changes in Hela cells following drug exposure were observed using light microscopy. The (**A**–**G**) graphs illustrate the alterations in cell shape observed following treatment with paclitaxel at concentrations between 0 and 100 nM, with (**H**,**I**) graphs providing further detail on the effects of 40 and 100 nM concentrations, respectively.

4. Conclusions

Through this research, we detected the inhibitory effects of paclitaxel on HeLa cells by combining terahertz (THz) spectroscopy with surface plasmon resonance (SPR) biosensors. The outcomes of the CCK-8 and MTT assays revealed a significant decrease in cell viability with increasing paclitaxel concentrations, indicating a dose-dependent effect. Optical microscopy further demonstrated that paclitaxel markedly altered the morphology and density of HeLa cells. The growth inhibition of HeLa cells became more pronounced at higher paclitaxel concentrations, aligning with other studies that have observed cell apoptosis under high-dose paclitaxel exposure. These findings provide new insights into paclitaxel's mechanism and offer a theoretical basis for its use in cancer treatment.

Furthermore, we utilized terahertz spectroscopy to non-invasively measure spectral changes in cells treated with varying concentrations of paclitaxel. The study revealed that the frequency of the terahertz absorption peaks significantly changed with increasing paclitaxel concentrations, indicating alterations in the dielectric constant within the cells. This change was negatively correlated with cell viability, further validating the potential of terahertz spectroscopy in studying drug–cell interactions.

Our study is the first to demonstrate that the utilization of terahertz spectroscopy in conjunction with SPR biosensors can rapidly and accurately evaluate the influence of medications on cancer cells. This novel approach not only provides a low-cost and efficient detection method but also offers a new technological platform for future research

on cancer drug screening and mechanism studies. The further optimization of this method, its application to other types of cancer cells and drugs, and the expansion of its application scope in biomedical research are potential avenues for future investigation.

Author Contributions: L.Z.: methodology, software, data analysis, writing—original draft and editing. G.C.: methodology, software, data analysis. Y.H.: investigation. Y.P.: funding acquisition, supervision, writing—review and editing. All authors have read and agreed to the published version of the manuscript.

Funding: This research was funded the National Key Research and Development Program of China (2022YFA1404004), the National Natural Science Foundation of China (61988102, 62335012), and the High-level Chinese Medicine Key Discipline Construction Project (ZYYZOKK-2023065) of the State Administration of Traditional Chinese Medicine.

Institutional Review Board Statement: Not applicable.

Informed Consent Statement: Not applicable.

Data Availability Statement: The data generated and analyzed during this study are available from the corresponding author upon reasonable request.

Conflicts of Interest: The authors confirm that there are no financial conflicts of interests or personal relationships that could have appeared to influence the work reported in this paper.

References

1. Sung, H.; Ferlay, J.; Siegel, R.L.; Laversanne, M.; Soerjomataram, I.; Jemal, A.; Bray, F. Global Cancer Statistics 2020: GLOBOCAN Estimates of Incidence and Mortality Worldwide for 36 Cancers in 185 Countries. *CA A Cancer J. Clin.* **2021**, *71*, 209–249. [CrossRef] [PubMed]
2. Cree, I.A.; White, V.A.; Indave, B.I.; Lokuhetty, D. Revising the WHO classification: Female genital tract tumours. *Histopathology* **2020**, *76*, 151–156. [CrossRef]
3. Lowy, D.R.; Solomon, D.; Hildesheim, A.; Schiller, J.T.; Schiffman, M. Human papillomavirus infection and the primary and secondary prevention of cervical cancer. *Cancer* **2008**, *113*, 1980–1993. [CrossRef] [PubMed]
4. Javeed, A.; Ashraf, M.; Riaz, A.; Ghafoor, A.; Afzal, S.; Mukhtar, M.M. Paclitaxel and immune system. European Journal of Pharmaceutical Sciences: Official. *J. Eur. Fed. Pharm. Sci.* **2009**, *38*, 283–290. [CrossRef] [PubMed]
5. De Furia, M.D. Paclitaxel (Taxol®): A new natural product with major anticancer activity. *Phytomedicine Int. J. Phytother. Phytopharm.* **1997**, *4*, 273–282. [CrossRef] [PubMed]
6. Dadgar, S.; Ramjan, Z.; Floriano, W.B. Paclitaxel is an inhibitor and its boron dipyrromethene derivative is a fluorescent recognition agent for botulinum neurotoxin subtype A. *J. Med. Chem.* **2013**, *56*, 2791–2803. [CrossRef] [PubMed]
7. Kampan, N.C.; Madondo, M.T.; McNally, O.M.; Quinn, M.; Plebanski, M. Paclitaxel and Its Evolving Role in the Management of Ovarian Cancer. *BioMed Res. Int.* **2015**, *2015*, 413076. [CrossRef] [PubMed]
8. Hong, X.; Li, S.; Li, W.; Wei, Z.; Guo, H.; Wei, W.; Zhang, S. Disruption of protein neddylation with MLN4924 attenuates paclitaxel-induced apoptosis and microtubule polymerization in ovarian cancer cells. *Biochem. Biophys. Res. Commun.* **2019**, *508*, 986–990. [CrossRef] [PubMed]
9. Punzi, S.; Meliksetian, M.; Riva, L.; Marocchi, F.; Pruneri, G.; Criscitiello, C.; Orsi, F.; Spaggiari, L.; Casiraghi, M.; Della Vigna, P.; et al. Development of Personalized Therapeutic Strategies by Targeting Actionable Vulnerabilities in Metastatic and Chemotherapy-Resistant Breast Cancer PDXs. *Cells* **2019**, *8*, 605. [CrossRef] [PubMed]
10. Mouradov, D.; Sloggett, C.; Jorissen, R.N.; Love, C.G.; Li, S.; Burgess, A.W.; Arango, D.; Strausberg, R.L.; Buchanan, D.; Wormald, S.; et al. Colorectal cancer cell lines are representative models of the main molecular subtypes of primary cancer. *Cancer Res.* **2014**, *74*, 3238–3247. [CrossRef]
11. Wilding, J.L.; Bodmer, W.F. Cancer cell lines for drug discovery and development. *Cancer Res.* **2014**, *74*, 2377–2384. [CrossRef]
12. Kim, H.; Lee, J.; Oh, C.; Park, J.H. Cooperative tumour cell membrane targeted phototherapy. *Nat. Commun.* **2017**, *8*, 15880. [CrossRef] [PubMed]
13. Adey, A.; Burton, J.N.; Kitzman, J.O.; Hiatt, J.B.; Lewis, A.P.; Martin, B.K.; Qiu, R.; Lee, C.; Shendure, J. The haplotype-resolved genome and epigenome of the aneuploid HeLa cancer cell line. *Nature* **2013**, *500*, 207–211. [CrossRef] [PubMed]
14. Carney, D.N.; Gazdar, A.F.; Bepler, G.; Guccion, J.G.; Marangos, P.J.; Moody, T.W.; Zweig, M.H.; Minna, J.D. Establishment and identification of small cell lung cancer cell lines having classic and variant features. *Cancer Res.* **1985**, *45*, 2913–2923. [PubMed]
15. Janckila, A.J.; Cardwell, E.M.; Yam, L.T.; Li, C.Y. Hairy cell identification by immunohistochemistry of tartrate-resistant acid phosphatase. *Blood* **1995**, *85*, 2839–2844. [CrossRef]
16. Zaynagetdinov, R.; Sherrill, T.P.; Kendall, P.L.; Segal, B.H.; Weller, K.P.; Tighe, R.M.; Blackwell, T.S. Identification of myeloid cell subsets in murine lungs using flow cytometry. *Am. J. Respir. Cell Mol. Biol.* **2013**, *49*, 180–189. [CrossRef]

17. Crisa, L.; McMaster, M.T.; Ishii, J.K.; Fisher, S.J.; Salomon, D.R. Identification of a thymic epithelial cell subset sharing expression of the class Ib HLA-G molecule with fetal trophoblasts. *J. Exp. Med.* **1997**, *186*, 289–298. [CrossRef]
18. Wang, R.; Wu, Q.; Zhang, Q.; Lu, Y.; Zhao, W.; Cai, W.; Qi, J.; Yao, J.; Xu, J. Conversion from terahertz-guided waves to surface waves with metasurface. *Opt. Express* **2018**, *26*, 31233–31243. [CrossRef]
19. Wang, Y.; Li, S.; Wang, H.; Tan, B.; Xiang, X.; Su, R.; Zhang, C.; Jin, B.; Chen, J.; Wu, P. Simple terahertz metasurface with broadband and efficient functionality. *Opt. Express* **2022**, *30*, 45488–45498. [CrossRef]
20. Sun, Y.; Huang, J.; Shan, L.; Fan, S.; Zhu, Z.; Liu, X. Quantitative analysis of bisphenol analogue mixtures by terahertz spectroscopy using machine learning method. *Food Chem.* **2021**, *352*, 129313. [CrossRef]
21. Shi, W.; Wang, Y.; Hou, L.; Ma, C.; Yang, L.; Dong, C.; Wang, Z.; Wang, H.; Guo, J.; Xu, S.; et al. Detection of living cervical cancer cells by transient terahertz spectroscopy. *J. Biophotonics* **2021**, *14*, e202000237. [CrossRef]
22. Shou, Y.; Wang, Y.; Miao, L.; Chen, S.; Luo, H. Realization of all-optical higher-order spatial differentiators based on cascaded operations. *Opt. Lett.* **2022**, *47*, 5981–5984. [CrossRef] [PubMed]
23. Liu, S.; Xu, F.; Zhan, J.; Qiang, J.; Xie, Q.; Yang, L.; Deng, S.; Zhang, Y. Terahertz liquid crystal programmable metasurface based on resonance switching. *Opt. Lett.* **2022**, *47*, 1891–1894. [CrossRef] [PubMed]
24. Chiang, W.F.; Silalahi, H.M.; Chiang, Y.C.; Hsu, M.C.; Zhang, Y.S.; Liu, J.H.; Yu, Y.; Lee, C.R.; Huang, C.Y. Continuously tunable intensity modulators with large switching contrasts using liquid crystal elastomer films that are deposited with terahertz metamaterials. *Opt. Express* **2020**, *28*, 27676–27687. [CrossRef] [PubMed]
25. Liu, B.; Peng, Y.; Jin, Z.; Wu, X.; Gu, H.; Wei, D.; Zhu, Y.; Zhuang, S. Terahertz ultrasensitive biosensor based on wide-area and intense light-matter interaction supported by QBIC. *Chem. Eng. J.* **2023**, *462*, 142347. [CrossRef]
26. Braun, K.; Stürzel, C.M.; Biskupek, J.; Kaiser, U.; Kirchhoff, F.; Lindén, M. Comparison of different cytotoxicity assays for in vitro evaluation of mesoporous silica nanoparticles. Toxicology in vitro: An international journal published in association with BIBRA. *Toxicol. Vitr.* **2018**, *52*, 214–221. [CrossRef]
27. Zhou, S.; Guo, P.; Li, J.; Meng, L.; Gao, H.; Yuan, X.; Wu, D. An electrochemical method for evaluation the cytotoxicity of fluorene on reduced graphene oxide quantum dots modified electrode. *Sens. Actuators B Chem.* **2018**, *255*, 2595–2600. [CrossRef]
28. Qin, H.; Liu, J.; Zhang, Z.; Li, J.; Gao, G.; Yang, Y.; Yuan, X.; Wu, D. In situ electrochemical assessment of cytotoxicity of chlorophenols in MCF-7 and HeLa cells. *Anal. Biochem.* **2014**, *462*, 60–66. [CrossRef] [PubMed]
29. Zhao, S.; Tang, Y.; Wang, R.; Najafi, M. Mechanisms of cancer cell death induction by paclitaxel: An updated review. *Apoptosis* **2022**, *27*, 647–667. [CrossRef]
30. Zhang, Y.; Tang, Y.; Tang, X.; Wang, Y.; Zhang, Z.; Yang, H. Paclitaxel Induces the Apoptosis of Prostate Cancer Cells via ROS-Mediated HIF-1α Expression. *Molecules* **2022**, *27*, 7183. [CrossRef]
31. Xie, K.; Liu, L.; Wang, M.; Li, X.; Wang, B.; Yin, S.; Chen, W.; Lin, Y.; Zhu, X. IMPA2 blocks cervical cancer cell apoptosis and induces paclitaxel resistance through p53-mediated AIFM2 regulation. *Acta Biochim. Biophys. Sin.* **2023**, *55*, 623–632. [CrossRef] [PubMed]